BNL-212070-2019-JAAM

Mechanochemical Nonhydrolytic Sol-Gel-Strategy for the Production of Mesoporous Multimetallic Oxides

Z. Zhang, S. Yang

To be published in "Chemistry of Materials"

August 2019

Energy Sciences Directorate

Brookhaven National Laboratory

U.S. Department of Energy

USDOE Office of Science (SC), Basic Energy Sciences (BES) (SC-22)

DISCLAIMER

CHEMISTRY OF MATERIALS

Article

pubs.acs.org/cm

Mechanochemical Nonhydrolytic Sol–Gel-Strategy for the Production of Mesoporous Multimetallic Oxides

Zihao Zhang,[†,‡,§] Shize Yang,[⊥] Xiaobing Hu,[#,▽] Haidi Xu,[§] Honggen Peng,[‡] Miaomiao Liu,[§] Bishnu Prasad Thapaliya,[§] Kecheng Jie,[§] Jiahua Zhao,[∥] Jixing Liu,[§] Hao Chen,[†] Yan Leng,[§] Xiuyang Lu,[†] Jie Fu,[*,†] Pengfei Zhang,[*,∥] and Sheng Dai[*,‡,§]

[†]Key Laboratory of Biomass Chemical Engineering of Ministry of Education, College of Chemical and Biological Engineering, Zhejiang University, Hangzhou 310027, P. R. China

[‡]Chemical Sciences Division, Oak Ridge National Laboratory, Oak Ridge, Tennessee 37831, United States

[§]Department of Chemistry, The University of Tennessee, Knoxville, Tennessee 37916, United States

[∥]School of Chemistry and Chemical Engineering, Shanghai Jiao Tong University, Shanghai 200240, P. R. China

[⊥]Center for Functional Nanomaterials, Brookhaven National Laboratory, Upton, New York 11973, United States

[#]Department of Materials Science and Engineering, Northwestern University, Evanston, Illinois 60208, United States

[▽]The NUANCE Center, Northwestern University, Evanston, Illinois 60208, United States

Supporting Information

ABSTRACT: Mesoporous metal oxides with wide pore size, high surface area, and uniform porous structures have demonstrated excellent advantages in various fields. However, the state-of-art synthesis approaches are dominated by wet chemistry, accompanied by use of excessive solvent, and the requirement of time-consuming drying process. Herein, we report a mechanochemical solid-state route to synthesize mesoporous Al_2O_3 (meso-Al_2O_3) via aluminum isopropoxide-copolymers assembly. The obtained meso-Al_2O_3 shows a record high surface area (~644 m^2 g^{-1}) and narrow pore size distribution (centered at ~5 nm). Moreover, a mechanochemical nonhydrolytic sol–gel strategy is introduced to fabricate mesoporous transition metal (Cu, Co, Mn, Fe, Mg, Ni)-aluminum binary oxide by using anhydrous metal chlorides and aluminum isopropoxide interplay. More importantly, four or five metals-aluminum oxide complexes with abundant mesopores and single cubic crystalline phase known as high-entropy ceramics are produced. To the best of our knowledge, mesoporous high-entropy metal oxides have not been prepared before, because the high crystallization temperature would make mesopores collapse. Additionally, this high-entropy property endows $(CuNiFeCoMg)O_x$–Al_2O_3 with superior SO_2-resisting performance (1000 ppm of SO_2 in N_2 at 280 °C) in the catalytic oxidation of CO compared to single CuO–Al_2O_3.

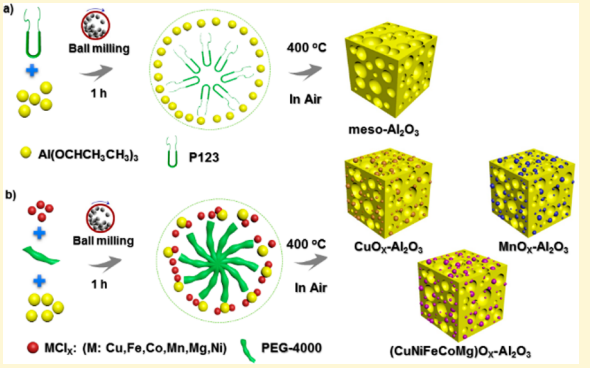

1. INTRODUCTION

Mesoporous metal oxides with wide pore size, high surface area, uniform pore size distribution, as well as a variety of structures and compositions endow them particularly attractive for applications in catalysis, adsorption, battery technology, sensing, and so on.[1−6] Template-assisted processes via either soft- or hard templates were usually used for the synthesis of mesoporous metal oxides.[7−12] In general, the hard-templating technique relied on mesoporous silica or carbon aerogel as the hard templates, which inevitably required additional steps and costs.[9,13−21] In comparison, organic–inorganic assembly routes, using block copolymers or surfactants as soft templates have been developed as a more straightforward method.[22−26] It is undeniable that the solvent evaporation-induced self-assembly method has been successfully applied into the synthesis of many mesoporous metal oxides.[27−29] However, several issues seem to remain in this wet soft-templating process, including: (1) excessive organic solvents are used; (2) it requires the metal precursors that have to be dissolved in the solvents, which limits the applications of many insoluble metal precursors;[3,30] and (3) the slow solvent evaporation is a time-consuming step.[31]

To resolve these disadvantages, solid-state synthesis, an old method in material processing, has been revisited.[32−35] Several porous materials, such as zeolite, metal–organic frameworks, covalent–organic frameworks, ordered mesoporous ploymers, and mesoporous carbons have been already synthesized via

Received: March 29, 2019
Revised: June 30, 2019
Published: July 1, 2019

DOI: 10.1021/acs.chemmater.9b01244
Chem. Mater. XXXX, XXX, XXX−XXX

mechanochemical processes.[36−38] Although a solvent-free assembly method has also been introduced for the construction of mesoporous metal oxide (TiO_2), this route needs HCl as the solvent and aged at 140 °C for 24 h before calcination, making it not a "true" solvent-free system.[37] As a result, the synthesis of mesoporous metal oxides via mechanochemical solid-state method, especially for metal oxdies hybrids, is highly welcome. Moreover, alumina has been widely used as an important carrier in catalysis, and alumina-based mixed mesoporous metal oxides also display extensive application prospect.[39−43] Therefore, the one-pot preparation of mesoporous alumina-supported metal oxides via mechanochemical solid-state method seems like a more efficient and straightforward pathway toward industrial catalysis.

Herein, we demonstrate the facile, rapid, and solid-state synthesis of mesoporous aluminum oxide (meso-Al_2O_3) by a mechanochemical assembly between aluminum isopropoxide and commercial polymers (e.g., PEO-PPO-PEO, P123; polyethylene glycol, PEO, PEG). Moreover, binary Al-based oxides (Cu, Co, Mn et al.) with abundant mesopores can be easily constructed by mechanochemical nonhydrolytic sol−gel process (NHSG, metal chlorides and aluminum isopropoxide interplay).[44−46] More interestingly, four or five transition metal species-aluminum oxide hybrids—the so-called high-entropy oxides—with single cubic crystalline phase and rich mesoporous structure were synthesized via this mechanochemical NHSG method. To our surprise, the high-entropy feature endows $(CuNiFeCoMg)O_x$−Al_2O_3 with superior SO_2-resisting performance (1000 ppm of SO_2 in N_2 at 280 °C) in the catalytic oxidation of CO compared to CuO−Al_2O_3.

2. EXPERIMENTAL SECTION

2.1. Catalyst Synthesis. *2.1.1. meso-Al_2O_3.* One gram of metal precursor (aluminum isopropoxide) and 0.2∼0.4 g soft templates (Pluronic P123:5800g mol^{-1}; PEG: 4000 g mol^{-1}, Pluronic F127 (F127), and cetyltrimethylammonium bromide (CTAB)) were added in a 9.5 mL screw-capped iron reactor with two big (diameter: 1.2 cm) and three small (diameter: 0.5 cm) iron steel ball bearings. The sealed reactor was placed in a high-speed vibrating ball miller (Retsch MM400), and the mixtures were ball milled for 60 min at a vibrational frequency of 30 Hz. The resulting samples were washed using ethanol and dried at 40 °C under vacuum conditions, followed by calcination at 400 °C with a heating rate of 2 °C min^{-1}.

2.1.2. Mesoporous Binary Metal Oxides (Cu, Co, and Mn et al.). Aluminum isopropoxide (2.67 mmol) and a transition metal chloride (4 mmol) as well as 0.4 g PEG were added in in a 9.5 mL screw-capped iron reactor with two big (diameter: 1.2 cm) and three small (diameter: 0.5 cm) iron steel ball bearings. After ball milling for 60 min, the post-treatment procedure is the same as that with the synthesis of meso-Al_2O_3. All catalysts were washed using water for three times before use.

2.1.3. $(CuNiFeCo)_x$−Al_2O_3. Aluminum isopropoxide (2.67 mmol), cooper chloride (1 mmol), nickel chloride (1 mmol), cobalt chloride (1 mmol), and ferrous chloride (1 mmol), as well as 0.4 g PEG are added in in a 9.5 mL screw-capped iron reactor with two big (diameter: 1.2 cm) and three small (diameter: 0.5 cm) iron steel ball bearings. After ball milling for 60 min, the post-treatment procedure is the same as that with the synthesis of meso-Al_2O_3.

2.1.4. $(CuNiFeCoMg)_x$−Al_2O_3. Aluminum isopropoxide (3.33 mmol), cooper chloride (1 mmol), nickel chloride (1 mmol), cobalt chloride (1 mmol), ferrous chloride (1 mmol), and magnesium chloride (1 mmol), as well as 0.4 g PEG are added in in a 9.5 mL screw-capped iron reactor with two big (diameter: 1.2 cm) and three small (diameter: 0.5 cm) iron steel ball bearings. After ball milling for 60 min, the post-treatment procedure is same with the synthesis of meso-Al_2O_3.

2.2. Characterizations. X-ray diffraction (XRD) was collected on a PANalytical Empyrean diffractometer operated at 45 kV and 40 mA (scanning step: 0.02° per step). N_2 adsorption−desorption isotherms were analyzed on a TriStar 3000 volumetric adsorption analyzer manufactured and by Micromeritics Instrument Corp. A classical Barrett−Joyner−Halenda (BJH) method was employed to determine the pore size distribution by using adsorption branch of isotherms. Prior to analysis, all samples were activated at 160 °C for 8 h. Scanning electron microscopy (SEM) with energy-dispersive X-ray spectroscopy (EDS) mapping results were recorded using a Zeiss EVO-MA15 scanning electron microscope with a Bruker XFlash 6130 detector. Scanning electron microscopy (SEM) images were recorded using a Zeiss AURIGA. Scanning transmission electron microscopy (STEM) was performed on a Nion microscope operated at 200 kV and ARM 200CF equipped with a probe corrector. The images are recorded using high angle annular dark field (HAADF) and bright field (BF) imaging. X-ray photoelectron spectroscopy (XPS) was performed by AXIS Ultra DLD spectrometer (Kratos, Japan). The obtained data were calibrated by C 1s standard peak and analyzed by Casa XPS software. Temperature-programmed desorption (TPD) of CO was recorded using FineSorb-3010 from Zhejiang Finetec Instruments Co., Ltd. with a thermal conductivity detector (TCD). Prior to characterization, fresh and spent catalysts were preheated at 120 °C under argon atmosphere. Elemental analysis of the samples was done by inductively coupled-plasma atomic emission spectroscopy (ICP-AES) using the Optima 2100 DV spectrometer (PerkinElmer Corporation). The actual metal ratios are summarized in Table S1 of the Supporting Information (SI). Fourier Transform infrared spectroscopy (FTIR) spectra were collected on a Bio-Rad FTIR spectrometer (Excalibur series).

2.3. Experimental Procedures. CO oxidation experiments were carried out in a fixed bed reactor (straight quartz tube with 4 mm inner diameter) at atmospheric pressure. For the measurement of CO light-off curves showing CO conversion as a function of reaction temperature, 20 mg of catalyst supported by quartz wool was loaded in the reactor. The feed gas of 1% CO balanced with dry air (<4 ppm water) passed though the catalyst bed at a flow rate of 10 mL/min corresponding to a gas hourly space velocity (GHSV) of 30 000 mL/(h g cat). The concentrations of CO and CO_2 in the reactor were analyzed by a Buck Scientific 910 gas chromatograph equipped with a dual molecular sieve/porous polymer column (Alltech CTR1) and a thermal conductivity detector. CO conversion is calculated as the peak areas of CO of consumption divided by that of CO before the reaction.

3. RESULTS AND DISCUSSION

Scheme 1 summarizes a mechanochemical route for the synthesis of meso-Al_2O_3 and related metal oxide hybrids using aluminum isopropoxide and anhydrous metal chlorides as the precursors, and P123 or PEG as the soft template. An efficient assembly between aluminum isopropoxide and P123 micelles is realized by mechanically grinding the mixture in a vibrating ball

Scheme 1. Synthesis of meso-Al_2O_3, Mesoporous Mixed Metal Oxides Using the Mechanochemical NHSG Method

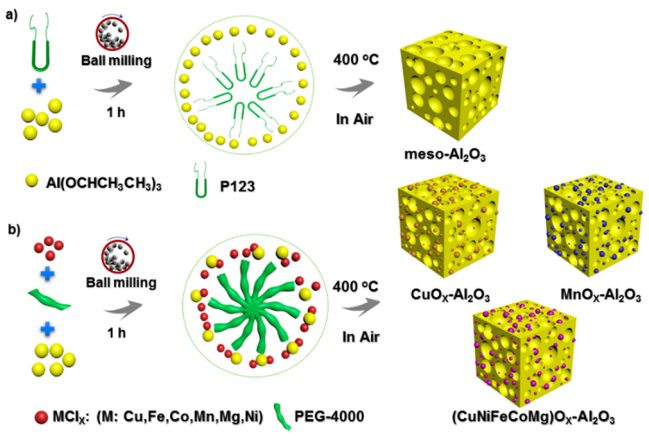

DOI: 10.1021/acs.chemmater.9b01244
Chem. Mater. XXXX, XXX, XXX−XXX

miller for 60 min (much shorter than the traditional solvent evaporation induced assembly process, 1−3 days in most cases).[23,47] It has been reported that the condensation between chloride and alkoxide by mixing the chloride precursors (MCl_x) and oxygen donor ($Al(OR)_3$) to produce the xerogels is considered to be an NHSG process.[48] The resulting xerogels are then washed and dried under vacuum and finally calcined in air to achieve the corresponding metal oxides. In this work, the mechanochemical NHSG process between metal chlorides and aluminum isopropoxide in the solid-state via complex mechanism is restricted to the periphery of micelles. The obtained xerogels are performed by XRD (Figure S1) and then calcinated at 400 °C in air to remove template. By combining with aluminum isopropoxide-copolymers cross-linking and NHSG process in one-step, the mixed oxides with uniform mesopores can be prepared.

The textural properties of the as-synthesized Al_2O_3 without and with different surfactants are summarized (Table 1) by N_2 adsorption−desorption isotherms at 77 K in Figure S2. The blank Al_2O_3 sample without templates offers a low surface area (246 m^2 g^{-1}) with a broad pore size distribution in Figure S2a,c. In comparison, a meso-Al_2O_3 sample with 0.2 g P123 as the template gives a type-IV isotherm with a H3-type hysteresis loop, resulting in both high surface area (415 m^2 g^{-1}) and narrow pore size distribution centered at ∼3 nm (Figure S2). For meso-Al_2O_3, a higher calcination temprature at 800 °C will lead to the collapse of a portion of the mesopores, as seen in Figure S3. Additionally, PEG, F127, and CTAB as templates also contribute to the formation of meopores smaller than 10 nm (Table 1). The weight ratio of P123/Al precursor exhibites signifcant influence for the formation of mesopores. The N_2 adsorption−desorption isotherms and pore size distrubution results of meso-Al_2O_3 synthesized with 0.4 g P123 displays a higher surface area of 644 m^2 g^{-1} and narrower pore size distribution of ∼5 nm (Figure 1a,b). It is nothworthy that the difference between the average pore size from Table 1 and the pore size distribution from Figure 1 should be ascribed to the limitation and accuracy of BJH model used. The transmission electron microscopy (TEM) and scanning transmission electron microscopy (STEM) image of meso-Al_2O_3 with 0.4 g P123 as the template also reveal the existence of a sponge-like nanoarchitecture with a large number of apparent mesopores (Figure 2a,b). A portion of mesopores is marked by yellow circles from STEM-EDS image in Figure S4. The wide-angle X-ray diffraction (XRD) result of meso-Al_2O_3 calcined at 400 °C with different templates shows an amorphous structure (Figures 3a and S5).

Table 1. Summary of Pore Parameter for Different Metal Oxides Calculated Using N_2 Adsorption−Desorption Isotherms at 77 K

samples	S_{BET} (m^2 g^{-1})	pore volume (cm^3 g^{-1})	average pore size (nm)
Al_2O_3	246	0.32	
meso-Al_2O_3 (0.4 g P123)	644	0.75	4.2
meso-Al_2O_3 (0.2 g PEG)	257	0.16	2.3
meso-Al_2O_3 (0.2 g CTAB)	380	0.26	
meso-Al_2O_3 (0.2 g F127)	329	0.24	
meso-Al_2O_3 (0.2 g P123)	415	0.34	2.6
CuO−Al_2O_3	115	0.11	2.8
Mn_3O_4−Al_2O_3	143	0.27	4.9
Co_3O_4−Al_2O_3	133	0.14	7.2
Fe_2O_3−Al_2O_3	178	0.24	5.8
NiO−Al_2O_3	168	0.15	3.3
MgO−Al_2O_3	176	0.18	6.3
(CuNiFeCo)O_x−Al_2O_3	129	0.13	3.9
(CuNiFeCoMg)O_x−Al_2O_3	198	0.24	4.8

[a]Specific surface area calculated using the BET equation. [b]Single point adsorption total pore volume of pores. [c]Average pore diameter from the distribution maxima by resolving adsorption branch with BJH model.

Compared with monometallic oxide, binary metal oxides tend to possess wider applications in catalysis. The traditional NHSG method for the production of metal oxides often takes place in organic solvents, and the corresponding pore size distribution is much wider.[46,48] By the mechanochemical NHSG route in the solid-state, mesoporous binary metal oxides (CuO-Al_2O_3, Mn_3O_4−Al_2O_3 and Co_3O_4−Al_2O_3) with uniform pore size distribution could be successfully synthesized with optimized PEG as the optimized template (Figures 1c−h and S6). In comparison to P123 and F127, PEG is a safe, inexpensive and renewable material. However, PEG has been used as soft templates with only limited success in directing mesopores until now. XRD results reveal the clear crystalline structures of CuO [JCPDS 44−0706], Mn_3O_4 [JCPDS 18−0803], and Co_3O_4 [JCPDS 43−1003] in CuO−Al_2O_3, Mn_3O_4−Al_2O_3, and Co_3O_4−Al_2O_3 samples, respectively (Figure 3a), and the corresponding crystalline sizes calculated by the Scherrer equation are 15.9, 13.4, and 11.8 nm, respectively. Additionally, no diffraction peaks associated with Al_2O_3 can be found in three binary metal oxides. Moreover, the diffraction peaks corresponding to NiO, MgO, and Fe_2O_3 crystalline phase, respectively, were discovered in the NiO−Al_2O_3, MgO−Al_2O_3, and Fe_2O_3−Al_2O_3 samples, respectively, as shown in XRD results (Figure S7).

The surface area and pore structure of CuO−Al_2O_3, Mn_3O_4−Al_2O_3, and Co_3O_4−Al_2O_3 were examined with N_2 adsorption−desorption isotherm measurements (Figure 1c,e,g). All samples show representative type-IV curves with clear capillary condensation steps between the relative pressure (P/P_0) of 0.4−0.8, underscoring the presence of rich mesopores. The specific surface areas of CuO−Al_2O_3, Mn_3O_4−Al_2O_3, and Co_3O_4−Al_2O_3 are 115, 144, and 133 m^2 g^{-1}, respectively (Table 1). More importantly, the pore size distributions by resolving the adsorption branch of N_2 isotherms with Barrett−Joyner−Halenda (BJH) method centered at 4, 6, and 7 nm for CuO−Al_2O_3, Mn_3O_4−Al_2O_3, and Co_3O_4−Al_2O_3, respectively (Figure 1d,f,h).[49] Moreover, N_2 adsorption and pore size distribution results of NiO−Al_2O_3, MgO−Al_2O_3, and Fe_2O_3−Al_2O_3 samples also reveal the existence of abundant mesoporous structure (Table 1; Figure S8). These obained abundant and uniform mesopores in binary metal oxides should be ascribed to solid-state self-assembly behavior of PEG micelles and different metal ions, confining NHSG process within the periphery of micelles. The results indicate that the mechanochemical NHSG route has the traits of universality for the preparation of a variety of binary metal oxides with uniform mesopore distributions. Additionally, the obtained surface area for both meso-Al_2O_3 and binary metal oxides are comparable to the previously reported mesoporous alumina and metal containing mesoporous alumina synthesized by conventional wet chemistry.[24,50]

Mn_3O_4−Al_2O_3 is then chosen as a representative to investigate the pore structure of binary metal oxides in a more tangible manner. Wormhole architectures with rich mesopores

DOI: 10.1021/acs.chemmater.9b01244
Chem. Mater. XXXX, XXX, XXX−XXX

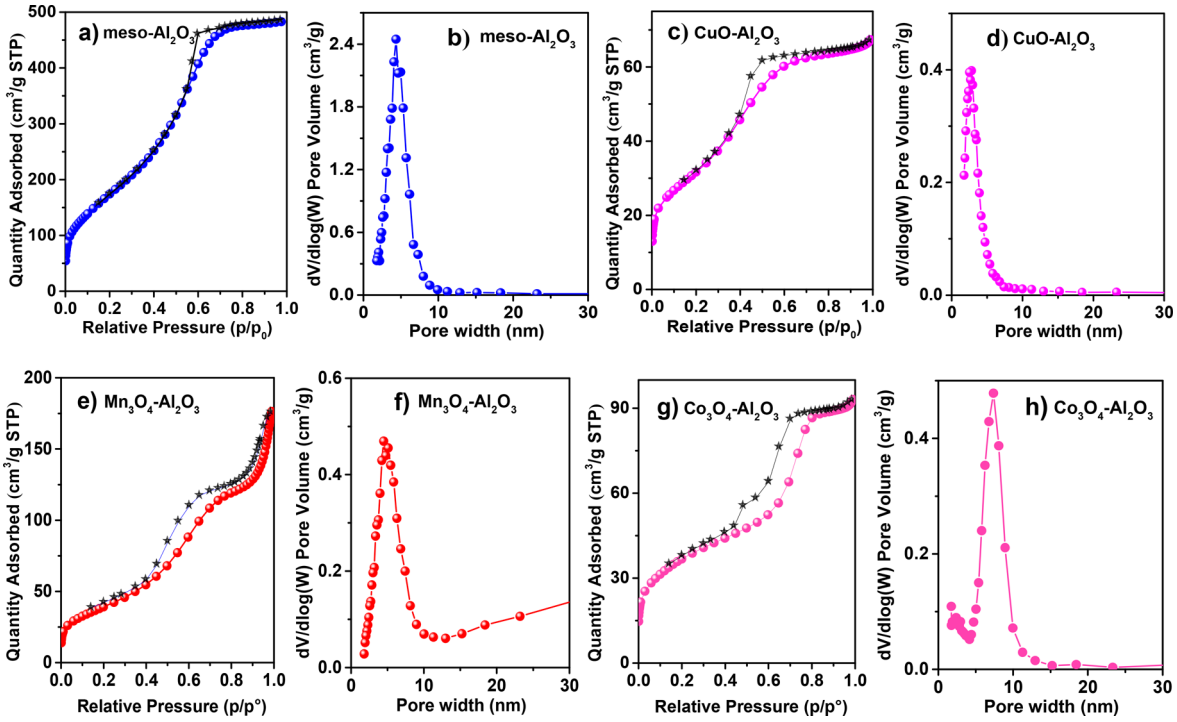

Figure 1. N_2 adsorption−desorption isotherms (a,c,e,g) and the corresponding pore size distribution (b,d,f,h) of meso-Al_2O_3, CuO−Al_2O_3, Mn_3O_4−Al_2O_3, and Co_3O_4−Al_2O_3 synthesized using a mechanochemical NHSG method.

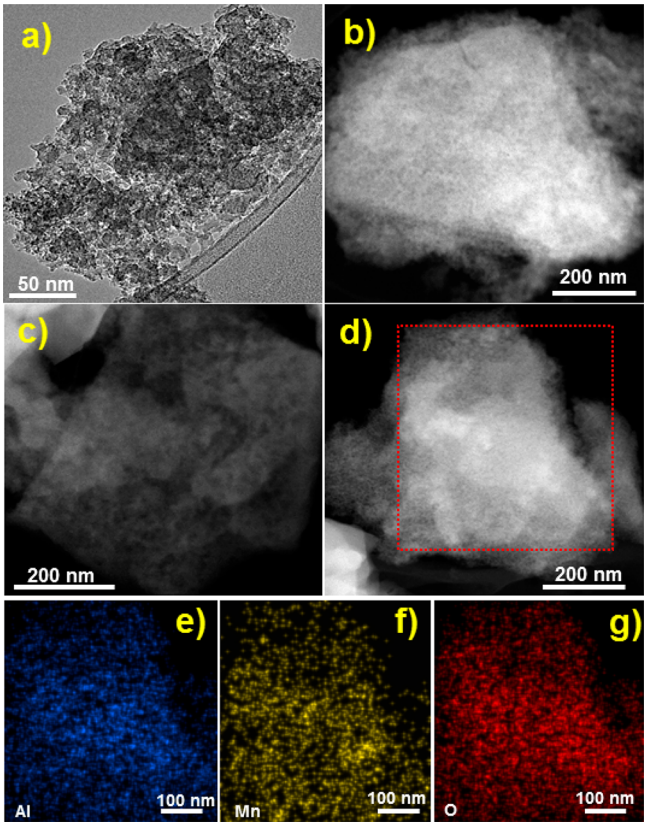

Figure 2. TEM a) and STEM-HADDF b) images of meso-Al_2O_3; STEM-HADDF images (c,d) of Mn_3O_4−Al_2O_3; and the corresponding element mapping signals e) Al, f) Mn and g) O.

side by side are observed throughout the material backbone in the range of several hundred nanometers (Figure 2c,d). Furthermore, energy-dispersive X-ray spectroscopy (EDS) mapping results of representative binary Mn_3O_4−Al_2O_3 sample (Figures 2e−g and Figure S9) show the well distribution of Mn, Al, and O, suggesting that the mesoporous structure is fabricated by the uniform mixture of Mn_3O_4 and Al_2O_3. Additionally, TEM and EDS-mapping results for CuO−Al_2O_3 and Co_3O_4−Al_2O_3 samples in Figures S10 and S11 also display existence of mesopores and unifrom mixture of CuO (Co_3O_4) and Al_2O_3.

Interestingly, the XRD result of (CuNiFeCo)O_x−Al_2O_3 sample synthesized by the same method does not show the characteristic diffraction peaks of CuO, Fe_2O_3, or Co_3O_4(Figure S12). The XRD pattern of (CuNiFeCo)O_x-Al_2O_3 reveals its crystalline structure, which is close to 37.2 (111), 43.3 (012), 62.8 (110), and 75.4 (113) reflections of cubic NiO (JCPDS 65-2901). The above results suggest that Cu, Fe, and Co may be incorporated into the sublattice of NiO to form a solid solution. STEM-HAADF images of (CuNiFeCo)O_x−Al_2O_3 sample reveal the aggregations of hybrid crystallites with a high degree of interstitial porosity (Figure 4a,b). EDS-mapping results show the highly uniform distribution of four metal species (Cu, Ni, Fe, and Co), further suggesting the existence of (CuNiFeCo)O_x solid solution (Figure S13). The pore nature of (CuNiFeCo)-O_x−Al_2O_3 sample was then evaluated via N_2 adsorption−desorption measurement at 77 K. A type-IV isotherm with an H_3 type hysteresis loop between the relative P/P_0 of 0.4 to 0.7 can be observed, leading to a surface area of 129 m^2 g^{-1} (Table 1) with narrow pore size distribution (~4 nm) (Figure 5a,b). The molar ratio of Al:(CuNiFeCo) obtained from ICP-AES result is 1.9, similar to 1.5 determined from EDS result in Figure S13.

Crystalline high-entropy metal oxides (normally containing five or more metal species), as a new class of material, have attracted great interest because of their unique structure and potential applications.[51,52] To date, the state-of-art high-entropy metal oxides only possess very limited surface area (e.g., < 30 m^2g^{-1}),[53,54] because their porous structures would collapse

DOI: 10.1021/acs.chemmater.9b01244
Chem. Mater. XXXX, XXX, XXX−XXX

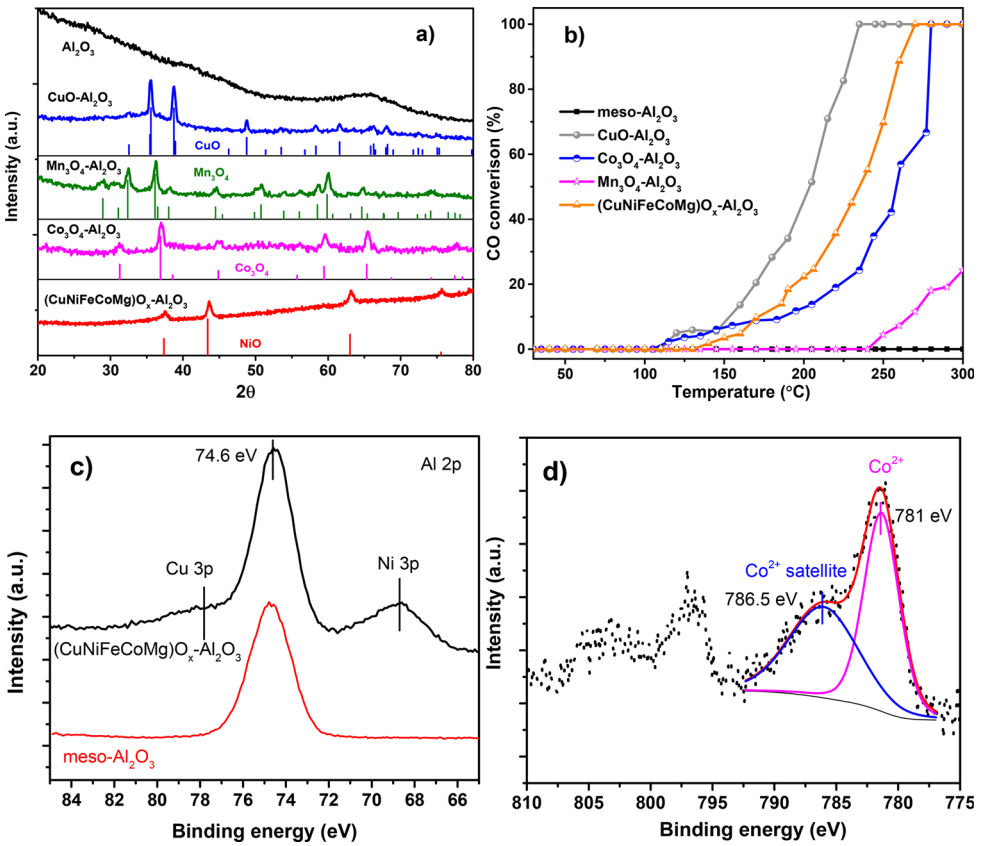

Figure 3. XRD results of a) meso-Al_2O_3, binary metal oxides and $(CuNiFeCoMg)O_x$–Al_2O_3; b) CO oxidation activity over different catalysts; normalized XPS spectra of c) Al 2p and d) Co 2p transitions for meso-Al_2O_3 (peak intensity for Al 2p is reduced) and $(CuNiFeCoMg)O_x$–Al_2O_3 samples.

during the removal of templates and the crystalllization process, which limits their performance in catalysis. To synthesize mesoporous high entropy metal–Al mixed oxides, Mg was chosen as the fifth metal element for the preparation of $(CuNiFeCoMg)O_x$–Al_2O_3. The basis for the choice of these metals is their similar atomic radius. The corresponding XRD patterns are displayed (Figure 3a). It is reassuring that when Mg is used as the fifth metal, the diffraction peaks become similar to the shift of diffraction peaks of cubic crystalline NiO. The diffraction peaks belonging to CuO, Fe_2O_3, Co_3O_4, and Mn_3O_4 in binary metal–Al oxides disappeared accidentally, suggesting the formation of single high-entropy phase). The crystalline size of high-entropy phase is approximately 11.6 nm determined by Scherrer equation. Moreover, SEM-EDS results reveal that five elements (Cu, Ni, Fe, Co, and Mg) signal are simultaneous discovered in selected regions (Figure 4e–l). The obtained results suggested that the high-entropy metal oxides $(CuNiFeCoMg)O_x$ should be formed and mixed uniformly with Al_2O_3 to form a mesoporous complex. We deduced that the mechanochemical process together with calcination step in are the major reason for the formation of solid solution.

The metal valence is illustrated by X-ray photoelectron spectroscopy (XPS) analysis, and the results are shown in Figures 3c,d and S14. The Al 2p XPS spectra in Figure 3c show the primary peak located at 74.6 eV for both meso-Al_2O_3 and $(CuNiFeCoMg)O_x$-Al_2O_3 samples, suggesting the existence of Al–O bonds in Al^{3+} (often known as Al_2O_3 species). The Cu 2p spectrum in Figure S14a can be fitted into four peaks, corresponding to Cu $2p_{3/2}$ (933.0 eV) and Cu $2p_{1/2}$ (953.0 eV) and their satellite peaks. These characteristics match well with standard peaks of CuO. The similar results in Ni 2p spectrum can identify the possible existence of NiO (Figure S14b).[55] The main peak from Mg 2p spectrum in Figure S14c is located around 50 eV, but the valence state of Mg is difficult to determine due to the close peak position of different state (Mg^0 and Mg^{2+}). However, Mg should exist in MgO form considering that the synthesis process is difficult to generate Mg^0. For Co 2p spectrum in Figure 3d, the peaks at 781 eV together with strong satellite at 786.5 eV indicate the existence of Co^{2+}, since the signature of Co^{3+} have no satellite peak.[56] The Fe 2p spectrum in Figure S14d suggests the coexistence of Fe^{2+} and Fe^{3+}.

STEM-HAADF images of $(CuNiFeCoMg)O_x$–Al_2O_3 sample suggest the existence of rich mesoporosity marked with small yellow circles (Figure 4c,d), which is also revealed by SEM images in Figure S15. The pore nature of $(CuNiFeCoMg)O_x$–Al_2O_3 sample was then evaluated by N_2 adsorption–desorption measurement at 77 K. A type-IV isotherm with steep adsorption peaks between the relative pressure (P/P_0) of 0.2–0.8, revealing the abundant mesoporous structure (Figure 5c,d). It offered a surface area up to 198 $m^2\ g^{-1}$, and the relatively lower surface area compared to meso-Al_2O_3 should be attributed to the blockage and collapse of pore channels during the crystallization process of high-entropy metal oxides. The molar ratio of Al: (CuNiFeCoMg) obtained from the ICP-AES result is 1.3.

Subsequently, the catalytic activities of different mesoporous metal oxides are evaluated for CO oxidation (Figure 3b). The T_{100} values (temperature for 100% CO conversion) are 220 °C (CuO–Al_2O_3), 270 °C (Co_3O_4–Al_2O_3), and 260 °C ($(CuNiFeCoMg)O_x$–Al_2O_3), respectively. Among these catalysts, Mn_3O_4–Al_2O_3 exhibits much worse activity for the

DOI: 10.1021/acs.chemmater.9b01244
Chem. Mater. XXXX, XXX, XXX–XXX

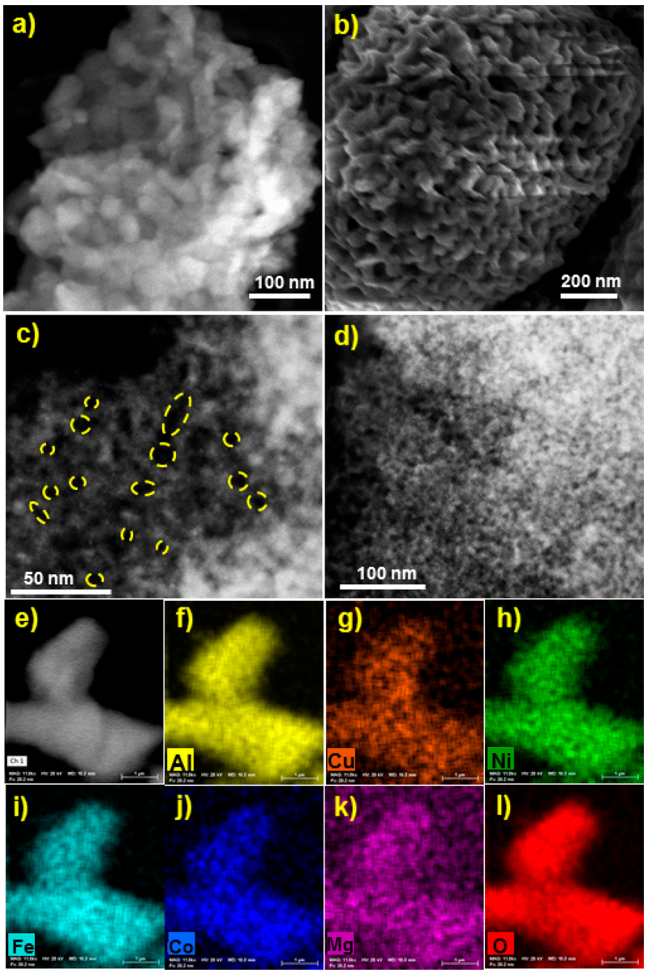

Figure 4. STEM (a) and SEM (b) images of $(CuNiFeCo)O_x$–Al_2O_3; STEM (c,d) images of $(CuNiFeCoMg)O_x$–Al_2O_3; SEM-EDS image (e) of $(CuNiFeCoMg)O_x$–Al_2O_3; and the corresponding element mapping signals f) Al, g) Cu, h) Ni, (i) Fe, j) Co, k) Mg, and l) O.

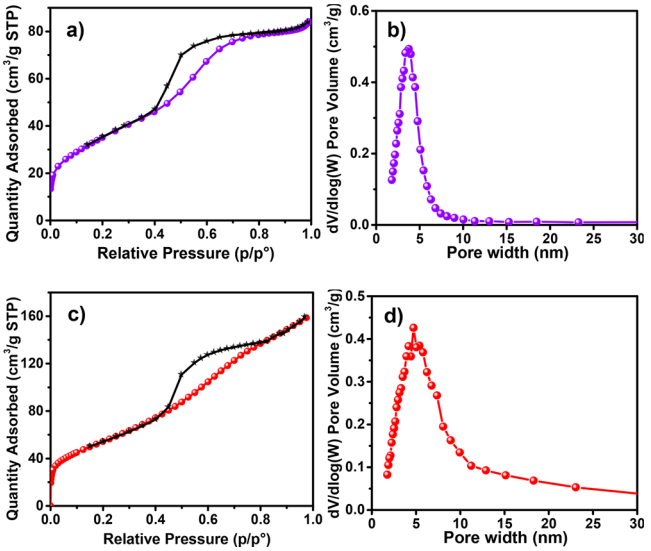

Figure 5. N_2 adsorption–desorption isotherms and the corresponding pore size distribution of $(CuNiFeCo)O_x$–Al_2O_3 (a,b) and $(CuNiFeCoMg)O_x$–Al_2O_3 (c,d) synthesized using mechanochemical NHSG method.

oxidation of CO, which may be attributed to the relatively inactive of Mn_3O_4 phase. And the mesoporous CuO–Al_2O_3 catalyst becomes active at 120 °C, and CO was completely converted at 220 °C, which are superior to most catalysts especially for Cu–Al mixed oxides prepared using traditional impregnation and precipitation method as shown in Table S2.[57−59] Moreover, both CuO–Al_2O_3 and $(CuNiFeCoMg)O_x$–Al_2O_3 catalysts exhibted remarkable stability even after being used for 48 h (Figure S16a,b). Considering the facile, fast, and solvent-free preparation method, these mesoporous mixed oxides may have great potential applications in industrial catalysis. As shown in Figure S17, XRD results of fresh and spent CuO–Al_2O_3 and $(CuNiFeCoMg)O_x$–Al_2O_3 catalysts display similar diffraction peaks and crystallite size. Additionally, temperature-programmed desorption (TPD) of CO in Figure S18 reveals similar CO desorption peak area, indicating the dispersion of metal active species does not decrease remarkably after use.

The sulfur tolerance is of great importance in real-world catalysis. However, CO oxidation activity of most catalysts went down remarkably in the presence of SO_2, greatly affecting the process of industrialization. Therefore, we compared the performance of SO_2 resistance over CuO–Al_2O_3 and $(CuNiFeCoMg)O_x$–Al_2O_3 catalysts. Before the catalytic activity test, each catalyst was treated in 1000 ppm of SO_2 at 280 °C for 5 h. The catalytic activity of CuO–Al_2O_3 decreased remarkably after SO_2 treatment (Figure S19a). It is noteworthy that there is a negligible effect of SO_2 on $(CuNiFeCoMg)O_x$–Al_2O_3 catalyst (Figure S19b). The decreased activity of CuO–Al_2O_3 is attributed to the formation of sulfites, evidenced by the feature in FTIR spectra around 1100 cm^{-1} (Figure S10).[60,61] However, it is clear that the formation of crystalline high-entropy metal oxides protect iteslf from SO_2 poisoning, contributing to the superior SO_2 tolerance compared with CuO–Al_2O_3. This result indicates that the $(CuNiFeCoMg)O_x$–Al_2O_3 catalyst may be stabilized by the relative higher configurational entropy, preventing itself from being sulfurated.[51]

4. CONCLUSIONS

In summary, an efficient, fast, and facile route for the synthesis of mesoporous Al_2O_3 and its metal oxide hybrids has been developed based on a mechanochemical nonhydrolytic method. The obtained meso-Al_2O_3 shows a record high surface area (~644 m^2 g^{-1}) and unifrom pore size (~5 nm). Moreover, mesoporous metal–aluminum oxide and four or five metal solid solution–aluminum oxide hybrids with rich mesoporous structure and single cubic crstalline phase was discovered. More importantly, this mechanochemical method does not need solvents and can shorten the pore filling process from 1–3 days to 60 min. The obtained mesoporous mixed metal oxide (such as $(CuNiFeCoMg)O_x$–Al_2O_3) exhibit not only an exceptional catalytic performance in CO oxidation, but also the superior SO_2 tolerance. This mechanochemical NHSG method may open the door to the scalable preparation of a new class of metal oxide catalysts.

■ ASSOCIATED CONTENT

Supporting Information

The Supporting Information is available free of charge on the ACS Publications website at DOI: 10.1021/acs.chemmater.9b01244.

DOI: 10.1021/acs.chemmater.9b01244
Chem. Mater. XXXX, XXX, XXX–XXX

Additional results of characterization results (XRD, SEM, TEM, N_2 adsorption−desorption, CO-TPD, ICP-AES, and FTIR) (PDF)

AUTHOR INFORMATION

Corresponding Authors

*E-mail: jiefu@zju.edu.cn.
*E-mail: chemistryzpf@sjtu.edu.cn.
*E-mail: dais@ornl.gov.

ORCID

Xiaobing Hu: 0000-0002-9233-8118
Haidi Xu: 0000-0002-6045-5600
Honggen Peng: 0000-0001-9133-5727
Hao Chen: 0000-0002-6658-4198
Yan Leng: 0000-0001-7618-0456
Xiuyang Lu: 0000-0002-6289-3110
Jie Fu: 0000-0002-3652-7715
Pengfei Zhang: 0000-0001-7559-7348
Sheng Dai: 0000-0002-8046-3931

Notes

The authors declare no competing financial interest.

ACKNOWLEDGMENTS

S.D. was supported by the Division of Chemical Sciences, Geosciences, and Biosciences, Office of Basic Energy Sciences, US Department of Energy. J.F. was supported by the National Natural Science Foundation of China (No. 21436007, 21706228), the Zhejiang Provincial Natural Science Foundation of China (No. LR17B060002). Z.Z. thanks the China Scholarship Council for financial support as a joint PhD student. P.F.Z. acknowledges Shanghai Pujiang Program (Grant No. 17PJ1403500), Thousand Talent Program, National Natural Science Foundation of China (Grant No. 21776174), and the Open Foundation of the State Key Laboratory of Ocean Engineering (Shanghai Jiao Tong University of China) (No. 1809) for the support.

REFERENCES

(1) Gu, D.; Schmidt, W.; Pichler, C. M.; Bongard, H. J.; Spliethoff, B.; Asahina, S.; Cao, Z.; Terasaki, O.; Schüth, F. Surface-casting synthesis of mesoporous zirconia with a CMK-5-like structure and high surface area. *Angew. Chem., Int. Ed.* **2017**, *56*, 11222.

(2) Gu, D.; Jia, C.-J.; Weidenthaler, C.; Bongard, H.-J.; Spliethoff, B.; Schmidt, W.; Schuth, F. Highly ordered mesoporous cobalt-containing oxides: structure, catalytic properties, and active sites in oxidation of carbon monoxide. *J. Am. Chem. Soc.* **2015**, *137*, 11407.

(3) Zhou, Y.; Antonietti, M. Synthesis of very small TiO_2 nanocrystals in a room-temperature ionic liquid and their self-assembly toward mesoporous spherical aggregates. *J. Am. Chem. Soc.* **2003**, *125*, 14960.

(4) Zhang, Z.; Zuo, F.; Feng, P. Hard template synthesis of crystalline mesoporous anatase TiO_2 for photocatalytic hydrogen evolution. *J. Mater. Chem.* **2010**, *20*, 2206.

(5) Ma, C. Y.; Mu, Z.; Li, J. J.; Jin, Y. G.; Cheng, J.; Lu, G. Q.; Hao, Z. P.; Qiao, S. Z. Mesoporous Co_3O_4 and Au/Co_3O_4 catalysts for low-temperature oxidation of trace ethylene. *J. Am. Chem. Soc.* **2010**, *132*, 2608.

(6) Liu, J.; Qiao, S. Z.; Hu, Q. H.; Max Lu, G. Q. Magnetic nanocomposites with mesoporous structures: synthesis and applications. *Small* **2011**, *7*, 425.

(7) Ko, Y. N.; Park, S. B.; Jung, K. Y.; Kang, Y. C. One-pot facile synthesis of ant-cave-structured metal oxide-carbon microballs by continuous process for use as anode materials in Li-ion batteries. *Nano Lett.* **2013**, *13*, 5462.

(8) Jin, Z.; Xiao, M.; Bao, Z.; Wang, P.; Wang, J. A general approach to mesoporous metal oxide microspheres loaded with noble metal nanoparticles. *Angew. Chem., Int. Ed.* **2012**, *51*, 6406.

(9) Xiao, W.; Yang, S.; Zhang, P.; Li, P.; Wu, P.; Li, M.; Chen, N.; Jie, K.; Huang, C.; Zhang, N.; Dai, S. Facile synthesis of highly porous metal oxides by mechanochemical nanocasting. *Chem. Mater.* **2018**, *30*, 2924.

(10) Li, W. C.; Lu, A. H.; Weidenthaler, C.; Schüth, F. Hard-templating pathway to create mesoporous magnesium oxide. *Chem. Mater.* **2004**, *16*, 5676.

(11) Gu, D.; Li, W.; Wang, F.; Bongard, H.; Spliethoff, B.; Schmidt, W.; Weidenthaler, C.; Xia, Y.; Zhao, D.; Schüth, F. Controllable synthesis of mesoporous peapod-like Co_3O_4@carbon nanotube arrays for high-performance lithium-ion batteries. *Angew. Chem., Int. Ed.* **2015**, *54*, 7060.

(12) Liu, H.; Li, W.; Shen, D.; Zhao, D.; Wang, G. Graphitic carbon conformal coating of mesoporous TiO_2 hollow spheres for high-performance lithium ion battery anodes. *J. Am. Chem. Soc.* **2015**, *137*, 13161.

(13) Zhen, M.; Zhou, B.; Ren, Y. Crystalline mesoporous transition metal oxides: hard-templating synthesis and application in environmental catalysis. *Front. Environ. Sci. Eng.* **2013**, *7*, 341.

(14) Malgras, V.; Ataee-Esfahani, H.; Wang, H.; Jiang, B.; Li, C.; Wu, K. C. W.; Kim, J. H.; Yamauchi, Y. Nanoarchitectures for mesoporous metals. *Adv. Mater.* **2016**, *28*, 993.

(15) Li, W.; Zhao, D. An overview of the synthesis of ordered mesoporous materials. *Chem. Commun.* **2013**, *49*, 943.

(16) Yang, H.; Zhao, D. Synthesis of replica mesostructures by the nanocasting strategy. *J. Mater. Chem.* **2005**, *15*, 1217.

(17) Lee, J.; Christopher Orilall, M.; Warren, S. C.; Kamperman, M.; DiSalvo, F. J.; Wiesner, U. Direct access to thermally stable and highly crystalline mesoporous transition-metal oxides with uniform pores. *Nat. Mater.* **2008**, *7*, 222.

(18) Ren, Y.; Ma, Z.; Bruce, P. G. Ordered mesoporous metal oxides: synthesis and applications. *Chem. Soc. Rev.* **2012**, *41*, 4909.

(19) Yue, W.; Zhou, W. Porous crystals of cubic metal oxides templated by cage-containing mesoporous silica. *J. Mater. Chem.* **2007**, *17*, 4947.

(20) Sun, X.; Shi, Y.; Zhang, P.; Zheng, C.; Zheng, X.; Zhang, F.; Zhang, Y.; Guan, N.; Zhao, D.; Stucky, G. D. Container effect in nanocasting synthesis of mesoporous metal oxides. *J. Am. Chem. Soc.* **2011**, *133*, 14542.

(21) Smått, J.-H.; Weidenthaler, C.; Rosenholm, J. B.; Lindén, M. Hierarchically porous metal oxide monoliths prepared by the nanocasting route. *Chem. Mater.* **2006**, *18*, 1443.

(22) Yang, P.; Zhao, D.; Margolese, D. I.; Chmelka, B. F.; Stucky, G. D. Generalized syntheses of large-pore mesoporous metal oxides with semicrystalline frameworks. *Nature* **1998**, *396*, 152.

(23) Zhang, Z.; Zhu, Y.; Asakura, H.; Zhang, B.; Zhang, J.; Zhou, M.; Han, Y.; Tanaka, T.; Wang, A.; Zhang, T.; Yan, N. Thermally stable single atom $Pt/m\text{-}Al_2O_3$ for selective hydrogenation and CO oxidation. *Nat. Commun.* **2017**, *8*, 16100.

(24) Yuan, Q.; Yin, A.-X.; Luo, C.; Sun, L.-D.; Zhang, Y. W.; Duan, W. T.; Liu, H. C.; Yan, C. H. Facile synthesis for ordered mesoporous γ-aluminas with high thermal stability. *J. Am. Chem. Soc.* **2008**, *130*, 3465.

(25) Feng, G.; Wang, J.; Boronat, M.; Li, Y.; Su, J. H.; Huang, J.; Ma, Y.; Yu, J. Radical-facilitated green synthesis of highly ordered mesoporous silica materials. *J. Am. Chem. Soc.* **2018**, *140*, 4770.

(26) Antonelli, D. M.; Ying, J. Y. Synthesis of hexagonally packed mesoporous TiO_2 by a modified sol-gel method. *Angew. Chem., Int. Ed. Engl.* **1995**, *34*, 2014.

(27) Zhou, W.; Li, W.; Wang, J.-Q.; Qu, Y.; Yang, Y.; Xie, Y.; Zhang, K.; Wang, L.; Fu, H.; Zhao, D. Ordered mesoporous black TiO_2 as highly efficient hydrogen evolution photocatalyst. *J. Am. Chem. Soc.* **2014**, *136*, 9280.

(28) Zhu, Y.; Zhao, Y.; Ma, J.; Cheng, X.; Xie, J.; Xu, P.; Liu, H.; Liu, H.; Zhang, H.; Wu, M.; Elzatahry, A. A.; Alghamdi, A.; Deng, Y.; Zhao, D. Mesoporous tungsten oxides with crystalline framework for highly sensitive and selective detection of foodborne pathogens. *J. Am. Chem. Soc.* **2017**, *139*, 10365.

DOI: 10.1021/acs.chemmater.9b01244
Chem. Mater. XXXX, XXX, XXX−XXX

(29) Li, Y.; Luo, W.; Qin, N.; Dong, J.; Wei, J.; Li, W.; Feng, S.; Chen, J.; Xu, J.; Elzatahry, A. A.; Es-Saheb, M. H.; Deng, Y.; Zhao, D. Highly ordered mesoporous tungsten oxides with a large pore size and crystalline framework for H_2S sensing. *Angew. Chem., Int. Ed.* **2014**, *53*, 9035.
(30) Wang, Y.; Yang, C. M.; Schmidt, W.; Spliethoff, B.; Bill, E.; Schüth, F. Weakly ferromagnetic ordered mesoporous Co_3O_4 synthesized by nanocasting from vinyl-functionalized cubic *Ia3d* mesoporous silica. *Adv. Mater.* **2005**, *17*, 53.
(31) Klimakow, M.; Klobes, P.; Thunemann, A. F.; Rademann, K.; Emmerling, F. Mechanochemical synthesis of metal-organic frameworks: a fast and facile approach toward quantitative yields and high specific surface areas. *Chem. Mater.* **2010**, *22*, 5216.
(32) Savateev, A.; Dontsova, D.; Kurpil, B.; Antonietti, M. Highly crystalline poly(heptazine imides) by mechanochemical synthesis for photooxidation of various organic substrates using an intriguing electron acceptor-Elemental sulfur. *J. Catal.* **2017**, *350*, 203.
(33) Cai, W.; Zhang, S.; Hu, X.; Jaroniec, M. In situ synthesis of nitrogen-enriched activated carbons from procambarus clarkii shells with enhanced CO_2 adsorption performance. *Energy Fuels* **2018**, *32*, 9701.
(34) Chen, D.; Zhao, J.; Zhang, P.; Dai, S. Mechanochemical synthesis of metal-organic frameworks. *Polyhedron* **2019**, *162*, 59.
(35) Zhao, J.; Shu, Y.; Zhang, P. Solid-state CTAB-assisted synthesis of mesoporous Fe_3O_4 and Au@Fe_3O_4 by mechanochemistry. *Chin. J. Catal.* **2019**, *40*, 1078.
(36) Jin, Y.; Sun, Q.; Qi, G.; Yang, C.; Xu, J.; Chen, F.; Meng, X.; Deng, F.; Xiao, F. S. Solvent-free synthesis of silicoaluminophosphate zeolites. *Angew. Chem., Int. Ed.* **2013**, *52*, 9172.
(37) Zhang, P.; Wang, L.; Yang, S.; Schott, J. A.; Liu, X.; Mahurin, S. M.; Huang, C.; Zhang, Y.; Fulvio, P. F.; Chisholm, M. F.; Dai, S. Solid-state synthesis of ordered mesoporous carbon catalysts via a mechanochemical assembly through coordination cross-linking. *Nat. Commun.* **2017**, *8*, 15020.
(38) Liu, F.; Huang, K.; Wu, Q.; Dai, S. Solvent-free self-assembly to the synthesis of nitrogen-doped ordered mesoporous polymers for highly selective capture and conversion of CO_2. *Adv. Mater.* **2017**, *29*, 1700445.
(39) Morris, S. M.; Fulvio, P. F.; Jaroniec, M. Ordered mesoporous alumina-supported metal oxides. *J. Am. Chem. Soc.* **2008**, *130*, 15210.
(40) Goncalves, A. A. S.; Costa, M. J. F.; Zhang, L.; Ciesielczyk, F.; Jaroniec, M. One-pot synthesis of $MeAl_2O_4$ (Me= Ni, Co, or Cu) supported on γ-Al_2O_3 with ultralarge mesopores: enhancing interfacial defects in γ-Al_2O_3 to facilitate the formation of spinel structures at lower temperatures. *Chem. Mater.* **2018**, *30*, 436−446.
(41) Gonçalves, A. A.; Jaroniec, M. Evaporation-induced self-assembly synthesis of nanostructured alumina-based mixed metal oxides with tailored porosity. *J. Colloid Interface Sci.* **2019**, *537*, 725−735.
(42) Goncalves, A. A. S.; Faustino, P. B.; Assaf, J. M.; Jaroniec, M. One-pot synthesis of mesoporous Ni-Ti-Al ternary oxides: highly active and selective catalysts for steam reforming of ethanol. *ACS Appl. Mater. Interface* **2017**, *9*, 6079−6092.
(43) Cai, W.; Yu, J.; Anand, C.; Vinu, A.; Jaroniec, M. Facile synthesis of ordered mesoporous alumina and alumina-supported metal oxides with tailored adsorption and framework properties. *Chem. Mater.* **2011**, *23*, 1147−1157.
(44) Tian, B.; Liu, X.; Tu, B.; Yu, C.; Fan, J.; Wang, L.; Xie, S.; Stucky, G. D.; Zhao, D. Self-adjusted synthesis of ordered stable mesoporous minerals by acid-base pairs. *Nat. Mater.* **2003**, *2*, 159.
(45) Debecker, D. P.; Bouchmella, K.; Poleunis, C.; Eloy, P.; Bertrand, P.; Gaigneaux, E. M.; Mutin, P. H. Design of SiO_2-Al_2O_3-MoO_3 metathesis catalysts by nonhydrolytic sol-gel. *Chem. Mater.* **2009**, *21*, 2817.
(46) Liu, Y.; Wang, M.; Li, Z.; Liu, H.; He, P.; Li, J. Preparation of porous aminopropylsilsesquioxane by a nonhydrolytic sol-gel method in ionic liquid solvent. *Langmuir* **2005**, *21*, 1618.
(47) Liu, H.; Li, Y.; Yin, C.; Wu, Y.; Chai, Y.; Dong, D.; Li, X.; Liu, C. One-pot synthesis of ordered mesoporous NiMo-Al_2O_3 catalysts for dibenzothiophene hydrodesulfurization. *Appl. Catal., B* **2016**, *198*, 493.
(48) Debecker, D. P.; Hulea, V.; Mutin, P. H. Mesoporous mixed oxide catalysts via non-hydrolytic sol-gel: a review. *Appl. Catal., A* **2013**, *451*, 192.
(49) Gunjakar, J. L.; Kim, T. W.; Kim, H. N.; Kim, I. Y.; Hwang, S. J. Mesoporous layer-by-layer ordered nanohybrids of layered double hydroxide and layered metal oxide: highly active visible light photocatalysts with improved chemical stability. *J. Am. Chem. Soc.* **2011**, *133*, 14998.
(50) Jiang, H.; Bongard, H.; Schmidt, W.; Schüth, F. One-pot synthesis of mesoporous Cu-γ-Al2O3 as bifunctional catalyst for direct dimethyl ether synthesis. *Microporous Mesoporous Mater.* **2012**, *164*, 3.
(51) Rost, C. M.; Sachet, E.; Borman, T.; Moballegh, A.; Dickey, E. C.; Hou, D.; Jones, J. L.; Curtarolo, S.; Maria, J. P. Entropy-stabilized oxides. *Nat. Commun.* **2015**, *6*, 8485.
(52) Sarkar, A.; Velasco, L.; Wang, D.; Wang, Q.; Talasila, G.; de Biasi, L.; Kubel, C.; Brezesinski, T.; Bhattacharya, S. S.; Hahn, H.; Breitung, B. High entropy oxides for reversible energy storage. *Nat. Commun.* **2018**, *9*, 3400.
(53) Chen, H.; Fu, J.; Zhang, P.; Peng, H.; Abney, C. W.; Jie, K.; Liu, X.; Chi, M.; Dai, S. Entropy-stabilized metal oxide solid solutions as CO oxidation catalysts with high-temperature stability. *J. Mater. Chem. A* **2018**, *6*, 11129.
(54) Sarkar, A.; Djenadic, R.; Usharani, N. J.; Sanghvi, K. P.; Chakravadhanula, V. S.; Gandhi, A. S.; Hahn, H.; Bhattacharya, S. S. Nanocrystalline multicomponent entropy stabilised transition metal oxides. *J. Eur. Ceram. Soc.* **2017**, *37*, 747.
(55) Zhang, Z.; Yang, Q.; Chen, H.; Chen, K.; Lu, X.; Ouyang, P.; Fu, J.; Chen, J. G. In situ hydrogenation and decarboxylation of oleic acid into heptadecane over a Cu-Ni alloy catalyst using methanol as a hydrogen carrier. *Green Chem.* **2018**, *20* (1), 197.
(56) Ovari, L.; Krick Calderon, S.; Lykhach, Y.; Libuda, J.; Erdohelyi, A.; Papp, C.; Kiss, J.; Steinruck, H.-P. Near ambient pressure XPS investigation of the interaction of ethanol with Co/CeO_2 (111). *J: Catal.* **2013**, *307*, 132.
(57) Nikolaev, S.; Golubina, E.; Krotova, I.; Shilina, M.; Chistyakov, A.; Kriventsov, V. The effect of metal deposition order on the synergistic activity of Au-Cu and Au-Ce metal oxide catalysts for CO oxidation. *Appl. Catal., B* **2015**, *168*, 303.
(58) Luo, M. F.; Fang, P.; He, M.; Xie, Y. L. In situ XRD, Raman, and TPR studies of CuO/Al_2O_3 catalysts for CO oxidation. *J. Mol. Catal. A: Chem.* **2005**, *239*, 243.
(59) Pantaleo, G.; Liotta, L.; Venezia, A.; Deganello, G.; Ezzo, E.; El Kherbawi, M.; Atia, H. Support effect on the structure and CO oxidation activity of Cu-Cr mixed oxides over Al_2O_3 and SiO_2. *Mater. Chem. Phys.* **2009**, *114*, 604.
(60) Goodman, A.; Li, P.; Usher, C.; Grassian, V. Heterogeneous uptake of sulfur dioxide on aluminum and magnesium oxide particles. *J. Phys. Chem. A* **2001**, *105*, 6109.
(61) Chen, F.-F.; Huang, K.; Fan, J. P.; Tao, D.-J. Chemical solvent in chemical solvent: a class of hybrid materials for effective capture of CO_2. *AIChE J.* **2018**, *64*, 632.

DOI: 10.1021/acs.chemmater.9b01244
Chem. Mater. XXXX, XXX, XXX−XXX